In-situ X-ray diffraction analysis of zirconia layer formed on zirconium alloys oxidized at high temperature

Dominique Gosset, Matthieu Le Saux

In-situ X-ray diffraction analysis of zirconia layer formed on zirconium alloys oxidized at high temperature

D. Gosset *, M. Le Saux

CEA, DEN, DMN, SRMA, 91191 Gif-sur-Yvette Cedex, France

In the case of a hypothetical loss of primary coolant accident (LOCA) in a light water reactor, the zirconium alloys fuel cladding would be oxidized in steam at high temperature, typically in the range 800–1200 ° C. The monoclinic to tetragonal phase martensitic transition of zirconia occurs within this temperature range and complex phenomena possibly having an impact on the oxidation kinetics are then to be expected. In order to provide an accurate description of the structure and microstructure of the oxide layers, systematic X-ray diffraction analyses have been performed in-situ under oxidizing atmosphere at high temperature (between 800 and 1100 °C) on Zircaloy-4 and M5™ sheet samples. It was confirmed that the volume fraction of the tetragonal and monoclinic zirconia phases formed during oxide growth drastically depends on the oxidation temperature. For example, the few outer microns of the oxide are fully tetragonal above 1050 °C and contain only 20% of tetragonal phase at 800 °C. It was also shown that cooling after oxidation induces irreversible phase transitions within the oxide. As a con-sequence, both the structure and the microstructure of the growing oxide cannot be observed post-facto, neither at room temperature nor after reheating at the prior oxidation temperature. It has been deduced from microstructural analyses that the grain size of the tetragonal zirconia phase is nanometric, about 100 nm during oxidation at 1100 °C down to 20 nm after cooling down to room temperature. This small grain size allows the stabilization of the tetragonal phase. The lattice parameters of the monoclinic and tetragonal zirconia phases have been analyzed, during both high temperature oxidation and cooling. In both cases, it appears the '*a*' and '*b*' cell parameters of the monoclinic phase are strongly constrained by the tetragonal '*a*' one. The structural characteristics of the oxide formed at high temperature on Zir-caloy-4 and M5™ are quite similar. All those results can be interpreted in the frame of the classical description of the monoclinic–tetragonal martensitic transition of zirconia.

1. Introduction

During a postulated loss of coolant accident (LOCA) in a Light Water Reactor (LWR), zirconium alloy fuel claddings would be oxidized in high temperature steam (typically between 800 and 1200 °C) and would then be embrittled. The oxidation kinetics of zirconium alloys are mostly sub-parabolic or parabolic at high temperature and the oxide layer is to some extent protective with respect to oxygen and hydrogen diffusion. But in some cases, a faster oxidation kinetics associated with a significant hydrogen uptake can be observed, then enhancing the cladding embrittlement. This is for example the case under high steam pressure (as encountered under intermediate break LOCA for Zircaloy-4 [1,2] and/or in post-breakaway oxidation conditions [3–5] at temperatures lower than 1050 °C. The breakaway oxidation occurs relatively suddenly during the oxidation. The shortest critical times, at which the breakaway oxidation transition takes place, are observed around 1000 °C. The mechanisms responsible for these changes of the oxidation kinetics, which depend on the oxidation temperature and the alloy in particular, are not fully understood so far but the monoclinic–tetragonal phase transition of zirconia is often mentioned [1,2,5]. Indeed in the temperature range of 800–1200 °C, pure zirconia undergoes a strongly first-order, martensitic phase transformation (monoclinic–tetragonal) [6] with a broad hysteresis and high cell distortions [7]. Complex structural and microstructural effects may then be inferred [8], with possible consequences on the oxide properties and the oxidation rate. Many studies have been devoted to the analysis of the monoclinic–tetragonal transition of zirconia. It appears the high temperature tetragonal phase can be stabilized at quite low temperatures down to room temperature when high stresses are applied to the oxide. These can originate from charged defects [9], surface energy in nanometric grains [10–12], irradiation effects [13] or pressure [14].

* Corresponding author. Tel.: +33 1 6908 5857; fax: +33 1 6907 7130.
E-mail address: dominique.gosset@cea.fr (D. Gosset).

Table 1
Composition (wt.%) of the studied zirconium-alloys.

	Sn	Fe	Cr	Nb	O
Zy4	1.3	0.22	0.11	–	0.12
M5™	–	0.04	–	1	0.14

In this framework, the characterization of the structure and the microstructure of the oxide growing at high temperature is an important issue, considering the effects on the oxidation rate of the material. The properties of the oxide formed at temperatures around 300 °C, typical of operational conditions in LWR, have been widely studied [15]. Such data are scarce for the oxide formed at higher temperature and structural characterizations are generally performed post-facto, i.e. after cooling down to room temperature or after re-heating in neutral atmosphere. However, recently published [16] preliminary high temperature X-Ray Diffraction (XRD) analyses performed on Zircaloy-4 samples exposed to an oxidizing atmosphere have clearly shown that reheating the samples to the oxidizing temperatures after cooling down to room temperature cannot reproduce the initial structure of the oxide. Furthermore, it has been observed that the phase composition of the oxide drastically depends on the oxidation temperature, e.g. the oxide is purely tetragonal at 1100 °C and mainly monoclinic at 800 °C.

This paper presents further results obtained on Zircaloy-4 and M5™[1] and aiming at an accurate description of those phenomena, i.e. the initial oxide phase composition versus the oxidation temperature within the 800–1100 °C range, the oxide stability during cooling and re-heating and the microstructural properties of the oxide.

2. Experimental procedures

The experiments have been performed on flat, 1 mm thick, 12 × 12 mm^2 squared sheet samples. It is then assumed the geometrical and metallurgical difference between a plate and a tube does not significantly affect the oxidation mechanisms. Two alloys have been studied, low-tin Zircaloy-4 (Zy4) and M5™. Their compositions are reported in Table 1. Zy4 is stress-relieved annealed, M5™ is fully recrystallized.

The facility already described in [16] was used. The XRD experiments were performed with an INEL-CPS120 multichannel detector. This allows the simultaneous recording of 120° 2θ diagrams (2θ being the angle of diffraction) on 4096 channels about 0.029° wide. This also leads to an asymmetric configuration. In that case, accurate tuning of the analyzed depth can easily be achieved by modifying the impinging angle of the incident X-ray beam on the sample. Here, a 5° incidence angle is chosen, for which 90% of the analyzed signal come from the outer 5 μm of the sample (with a low difference between the metal and the oxide). Conversely, it is worth noting that, due to the X-ray absorption in the materials, the method does not make it possible to analyze the actual composition at the metal–oxide interface when the oxide thickness is higher than around 5 μm [17]. One must then assume that the subsequent modifications of the oxide that have been observed, e.g. during cooling, do not significantly depend on the oxide thickness. This is an obvious limitation of the method. Moreover, in this asymmetric configuration, the orientation of the diffraction vector to the surface of the sample depends on the (hkl) lines: the different lines then correspond to different orientations of the diffracting grains and the results cannot easily be compared to e.g. Bragg–Brentano analyses [18].

The incident beam is made parallel and purely monochromatic (Cu Kα_1) with a Ge (1 1 1) single crystal monochromator. A selection window leads to an 80 μm × 6 mm beam size: at a 5° incidence, the illuminated area on the sample is then around 1 mm wide. The analyses were performed in an Anton-Paar HTK-1200 furnace with a 190° window that has been specifically modified for the CPS120 detector. The window is closed with a 0.3 mm thick kapton foil protected with a 20 μm thick Ni foil: both contribute to the diffraction patterns (extra lines), but with no consequence on the metal and oxide diagrams. The furnace holder is motorized in order to adjust the height and the incidence of the sample relatively to the incident X-ray beam. The height was automatically tuned to compensate the sample holder thermal expansion when necessary. The temperature was measured with a thermocouple close the sample. A calibration has been performed to correct the difference between the temperature measured by the thermocouple and the actual sample temperature. Qualitative analyses, allowing phase identification, were performed on the basis of 30 s diagram recording. Microstructural analyses require longer recording times, here 500 s.

A gas circuit allows the introduction into the furnace of two different gas with a controlled flow (atmospheric pressure), in the present case an inert gas (6 N He, pO_2 < 5 ppm) and a 60 vol.% He–40 vol.% O_2 mixture (used as an acceptable surrogate for steam). Helium has been chosen as a buffer gas in order to improve the thermal conductivity of the oxidizing atmosphere and avoid any significant temperature overshoot at the beginning of the exothermic oxidation of the sample. A zirconia probe (Systech 800 serial 820 type, O_2 sensitivity 0.1 vol ppm) has been added to the exit of the gas circuit in order to measure the oxygen partial pressure, in particular during heating in inert atmosphere.

The experiments aim first at observing the oxide phases forming on the metal surface. The metal surface becomes nearly invisible when the oxide thickness is over a few micrometers. Therefore, in order to analyze the oxide that is growing at high temperature and not the oxide formed during heating, the sample must be nearly non-oxidized when the oxidation temperature is reached. For that, the samples were first heated in inert atmosphere (low gas flow, 30 cm^3/min) then oxygen was introduced when the target oxidation temperature (800–1100 °C) was reached. The samples were then maintained at the oxidation temperature until disappearance of the metal on the diagrams. As shown in Fig. 1, a transitory stage was observed during heating under 6N–He, between circa 400 °C and 1000 °C: a zirconia layer with a thickness of a

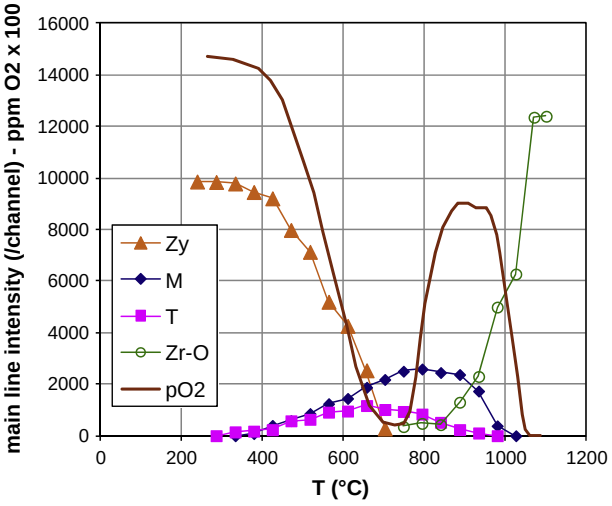

Fig. 1. Intensity of the main line of the phases observed on a Zy4 sample heated under 6N–He atmosphere. A few micrometers thick oxide layer first forms then disappears above 900 °C. Zy: Zy-4; M: monoclinic ZrO_2; T: tetragonal ZrO_2; Zr–O: α-Zr(O); pO_2: O_2 partial pressure, ppm × 100.

[1] M5™ is a trademark of Areva NP registered in the USA and in other countries.

few micrometers (as deduced from the attenuation of the metal diagram) starts to form from about 300 °C on the metal surface (the very low oxygen content of the used inert gas is sufficient to slightly oxidize the material) then progressively disappears from about 900 °C. The dissolution of the former oxide layer is associated with oxygen diffusion into the metallic substrate [19] and results from the progressive reduction of the oxygen partial pressure in the atmosphere and the low incoming oxygen flux at the metal surface (oxidation of zirconium alloys mainly occurs by anion diffusion from the environment to the metal/oxide interface where the chemical reaction takes place).

This oxide layer formed during heating under 6N He is biphasic, monoclinic (M) and tetragonal (T). Since the T phase disappears before the M phase when the metal reappears, the T phase of zirconia is most probably located at the metal–oxide interface (obviously the transformation of T to M cannot occur since the temperature is increasing), as usually observed due to higher stress levels at this location [20]. In the meanwhile, oxygen has diffused into the metallic substrate and, in the 700–800 °C temperature range, the metal just beneath the oxide has transformed from the α-Zr phase to an oxygen-saturated α-Zr(O) phase (oxygen content up to about 7 wt.% or 29 at.%) [21]. α-Zr and α-Zr(O) have both a hexagonal structure but they have slightly different cell parameters values: Fig. 2. The cubic high temperature β-Zr phase was not observed on the measured diagrams for the investigated conditions because, when it is present, this phase is located below the α-Zr(O) phase layer and the depth analyzed by XRD is limited to about 5 μm with the chosen incidence angle. The evolution of the partial oxygen pressure during heating under 6N–He shows three stages: it decreases when the metal is oxidizing, increases when the oxide layer slows down the oxygen diffusion rate to the metal, decreases down to nearly zero (<0.1 vol ppm) when the oxide layer is completely reduced and the metal reappears on XRD diagrams.

The main purpose of this work was to determine the microstructural parameters of the oxide, but also the fractions of the oxide phases when biphasic. This issue is quite challenging. The main difficulty is that the material is highly textured, due to the nucleation and growing processes of the oxide layer, the stresses induced by the underlying textured metal and the steric relations between the different oxide phases [22]. Moreover, the texture of the oxide is not fiber-like, leading to different diagrams when the recordings are made according to different orientations of the initial metal sample. At last, the classical texture correction procedures, such as the Marsch–Dollase one, cannot be used in the case of an asymmetric setup [18] since the diffraction vector turns depending on the considered reflection. Here, to cope with this difficulty, different methods were used. First, the simplest and most widely used method is based on the ratio of the intensity of the main lines of the oxide phases, namely the $(\bar{1}11)_M$ and $(111)_M$ monoclinic lines and the $(101)_T$ tetragonal one:

$$\frac{T}{T+M} = \frac{(101)_T}{(101)_T + (\bar{1}11)_M + (111)_M}$$

where T and M stand for tetragonal and monoclinic.

In some cases, it was possible to analyze the diagrams with the so-called full-pattern-matching (FPM) method. The phases proportions are then obtained by the ratio of the integral intensities of each diagram, here neglecting the density difference between the T and M zirconia phases and the texture effects due to the asymmetric setup. Those two evaluations are compared on Fig. 3 in the case of a Zy4 sample oxidized at 1100 °C then cooled down (with 500 s long steps every 25–100 °C for diagram recording) to room temperature (under oxidizing atmosphere). It appears the two methods lead to the same evaluations when one phase is dominant. However, in the biphasic domain significant differences arise, leading to an apparent shift on the transition of about 30 °C. It is worth noting that it is impossible to determine which the best method is. This is clearly a limitation of the evaluations performed by XRD in such systems [23]. The FPM method also shows the texture of the oxide phases is modified during cooling. The consequence is that the sum of the intensity of the diagrams is not constant in that temperature range.

3. Results

3.1. Phase composition and stability of the oxides versus oxidizing temperature

On a first step, XRD analyses were performed during high temperature isothermal oxidation in the 1100–800 °C range then during slow cooling to room temperature under low helium–oxygen flow. Diagrams recording during cooling was performed every 25 °C with 500 s long plateaus. The samples were then re-heated

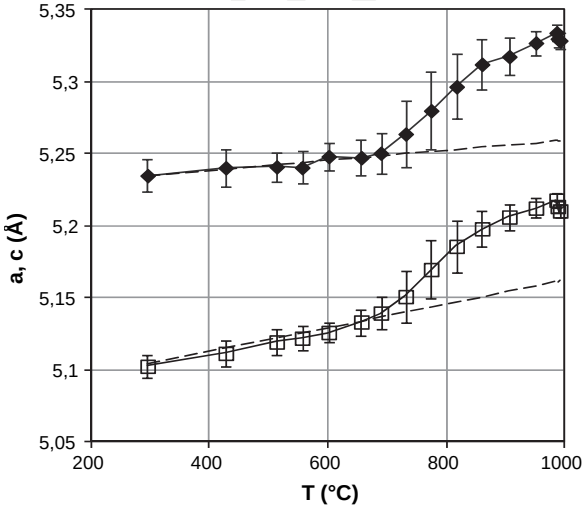

Fig. 2. Cell parameters of the metal phases during heating in 6N–He atmosphere. ♦: a ($\times\sqrt{(8/3}$ for visibility, c/a ratio for the ideal hexagonal compact structure). □: c. --- : linear extrapolation of low temperature variations.

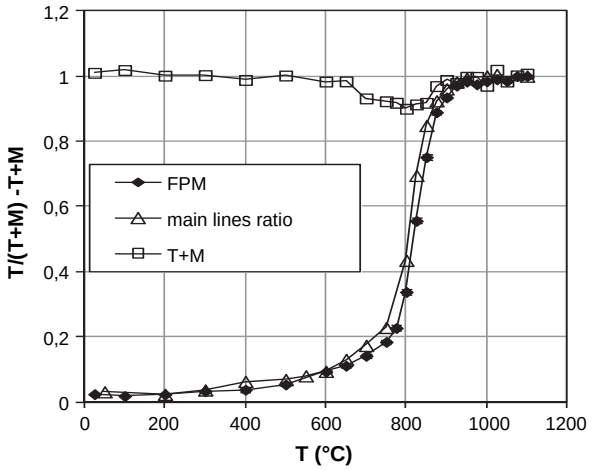

Fig. 3. Relative proportion of T ZrO_2 during cooling of a Zy4 sample oxidized at 1100 °C, estimated with two methods. △: ratio of main lines intensities. ♦: FPM method on the whole diagrams (Section 3.2). T + M: total relative intensity (FPM evaluation).

to the former oxidation temperature under 6N–He and diagrams were recorded every 100 °C. Here the oxide phases proportion is estimated from the intensity of the main lines.

In all cases, only the tetragonal and monoclinic phases of zirconia were identified (the cubic phase was not observed). In the studied oxidation temperature range, i.e. 800–1100 °C, the oxide growth is very fast (by comparison to the oxide growth rate under operational conditions in LWR for example): the metal disappears from the diagrams in less than 30 s, meaning that the oxide thickness is higher than 5–10 μm. The oxides formed are highly textured, making the classical Rietveld diagrams analyses impossible.

For the samples oxidized at 1100 °C, only the tetragonal ZrO_2 phase appears. A sharp transition occurs around 850 °C during cooling from the oxidation temperature and only a small residue of the tetragonal ZrO_2 phase remains at room temperature (Figs. 4 and 5). This allows an accurate analysis of each phase by full-pattern-matching as it will be discussed in the next section. When re-heated at 1100 °C, the oxide still appears to be mainly monoclinic (Fig. 6).

For oxidation temperatures lower than or equal to 1050 °C, the oxide is biphasic. The fraction of the tetragonal phase decreases when the oxidation temperature is made to decrease but, the lower the oxidation temperature, the higher the tetragonal phase proportion at room temperature (Fig. 4). Conversely, when reheated at the oxidation temperature, the higher the oxidation temperature and the lower the final tetragonal phase proportion. This clearly confirms that the structure of the oxide formed at high temperature is irreversibly modified during cooling and cannot be recovered by re-heating the samples to the oxidation temperature.

Quite similar results have been obtained for the two studied alloys, Zy4 and M5™. Nevertheless, the T to M phase transition during cooling after oxidation at 1100 °C appears to be sharper and occurs at a temperature somewhat higher (about 50 °C) in the case of M5™ by comparison to Zy4 (Fig. 4): this might indicate slight microstructural differences between the oxides on the two alloys.

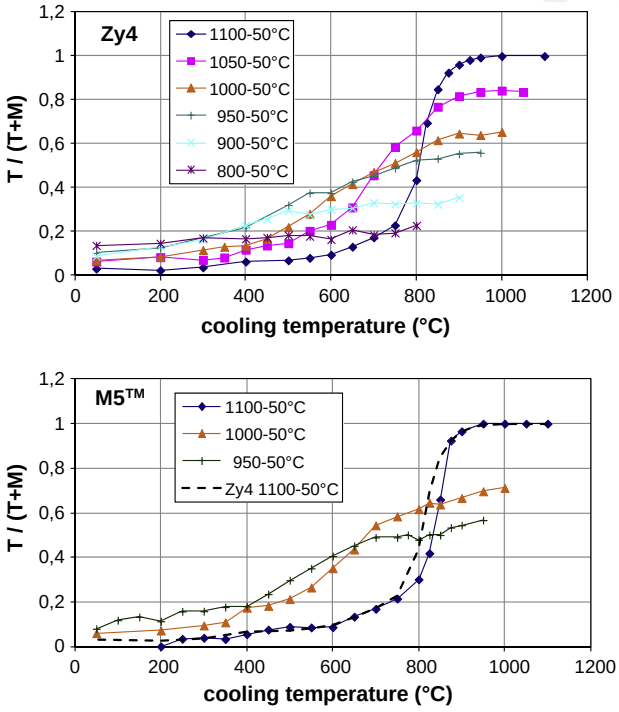

Fig. 4. Proportion (evaluated from the ratio of the main lines intensities) of tetragonal zirconia forming on zirconium alloys oxidized at temperatures between 800 °C and 1100 °C then cooled down to room temperature. Top: Zy4 alloy. Bottom: M5™ alloy.

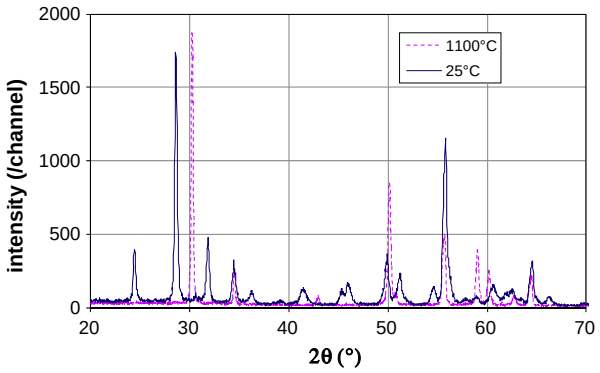

Fig. 5. Diffraction diagrams of the surface oxide of a Zy4 sample oxidized at 1100 °C. At 1100 °C (dotted fuchsia line), the oxide is purely tetragonal. When cooled at 25 °C (blue line), it is nearly purely monoclinic (small $(10\bar{1})_T$ line at 30°) and highly textured. (For interpretation of the references to colour in this figure legend, the reader is referred to the web version of this article.)

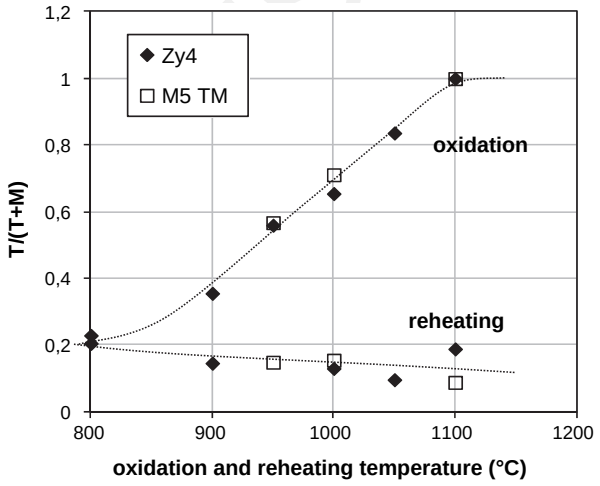

Fig. 6. Proportion of tetragonal zirconia (evaluated from the ratio of the main lines intensities) as a function of the oxidation temperature. Oxidation: at the oxidation temperature. Re-heating: when reheated at the oxidation temperature after cooling down to room temperature. ♦: Zy4. □: M5™.

3.2. Microstructural properties of the oxide formed at 1100 °C

Full-pattern-matching analyses of the diagrams have been performed for the Zy4 sample oxidized at 1100 °C. In that case, only the tetragonal phase appears on the diagrams recorded during oxidation at high temperature. This allows a non-ambiguous identification of the lines (Fig. 5). Therefore it becomes possible to perform an accurate analysis of the cell parameters and the diffraction lines profiles. Similarly, the tetragonal phase has a very low intensity on the diagrams obtained at room temperature after cooling (Fig. 5). This residue can then be approximated from the diagram obtained at high temperature for the tetragonal phase by assuming that the relative intensities of the lines are similar so that only the cell parameters and line profile have to be adjusted. The monoclinic phase diagram can then be fitted by the same method, leading to an accurate determination of the same microstructural parameters for the monoclinic phase.

Afterward, by assuming there is no significant evolution as a function of the temperature of the orientations of the zirconia

grains, these two reference diagrams for the tetragonal and monoclinic zirconia phases have been propagated, from high temperature and room temperature respectively, over the whole set of diagrams recorded at intermediate temperatures. This then allows the determination of the cell parameters and the line profile parameters for each phase. This analysis has been performed by using the XND Rietveld program [24] that has been modified in order to take into account the specific geometrical corrections induced by the asymmetric setting of the goniometer [25].

The evolution during cooling from 1100 °C of the phase composition of the surface oxide is reported in Fig. 3 (T/(T + M) curve). The evolution of the cell parameters are reported in Fig. 7. The β angle of the monoclinic phase increases quickly between 900 °C (highest temperature allowing fitting) and 600 °C from 98.6° to 98.9°, then slower up to 99.1° at 25 °C. The fitting agreement appears to be poor during the T to M phase transition (Rbragg factor, which provides an indication of the quality of the description of the phases, higher than 15% [26]) and the total intensity of the monoclinic and tetragonal phases diagrams is not constant. This means that the relative intensities of the lines should change during cooling. This has been checked for a few main lines on the diagrams obtained at 850 °C and 800 °C. For example, the relative intensity of the $(0\,1\,1)_M$ line is 0.49 at 850 °C and 0.26 at 800 °C; for the $(1\,0\,3)_T$ line, it is 0.25 at 850 °C and 0.18 at 800 °C. Therefore the orientations of the new and the former zirconia grains are different.

On the diffraction diagrams, the position of the lines depends on the cell parameters of the material and on the centering of the sample relatively to the center of the goniometer. All those parameters are simultaneously refined by the Rietveld program. In the present case, the offset from the goniometer center is low (about 0.1 mm) with a uniform evolution during cooling. As a consequence, the cell parameters evolutions to be observed are not affected by geometrical systematic errors. The a parameter of the monoclinic phase (a_M) is equal to the a parameter of the tetragonal phase (a_T), modulo the $\sqrt{2}$ and $\sin\beta$ geometrical corrections, on the whole investigated temperature range. In the same way, the a and b parameters of the monoclinic phase are nearly equal when this phase appears during cooling. They then evolve to reach the usual a/b ratio when the tetragonal phase fraction becomes low. At last, the c parameter of the residual tetragonal phase (c_T) is nearly equal to the b parameter of the monoclinic phase below 500 °C. This means strong topotaxic constraints exist between the two phases [27]. In the high temperature range, where the tetragonal phase is alone, the change of the cell parameters during cooling is larger than the change that would solely result from thermal contraction (steeper evolution than at low temperature). This could be induced by relaxation effects, due to an increase of the oxide thickness and/or to creep of the underlying metal at high temperature, or under the effect of the oxidation-induced stresses resulting from the volume change associated with the formation of the oxide and from oxygen dissolution and diffusion in the metal substrate. Dimensional changes of the sample were observed, illustrating the plastic deformation of the metal and eventually of the oxide during the experiments. In the 900–700 °C range, where both zirconia phases are present in significant proportions, the cell parameters show unusual evolutions, with plateaus or increase with decreasing temperature. Such an evolution, different from the continuous contraction expected during cooling, can be explained by assuming that the initial high stresses within the outer oxide relax during the T to M phase transformation. The T to M phase transition is accompanied by a volume increase so that an increase of compressive stresses within the oxide may be expected but stress relaxation can occur as a result of the viscoplastic deformation of the metal and the oxide, the β-Zr to α-Zr phase transformation, the thermal contraction differentials between the different phases and/or the formation of pores and micro-cracks in the oxide.

In order to fit the material components to the linewidths, the XND program uses the classical $1/\cos\theta$ and $\tan\theta$ functions, which respectively correspond to the size of coherent diffraction domains (CDD) and to the micro-strain components of the so-called Hall–Williamson analysis [7]. On the one hand, it was observed that the micro-strain component is low, meaning that the crystals are homogeneous and low defective. On the other hand (Fig. 8), the size of the CDD of the tetragonal phase is around 110 nm at high temperature (1100 °C), sharply decreases to 20 nm during the T to M transition down to about 700 °C and finally remains constant down to room temperature. The first monoclinic phase domains also have a size of about 110 nm. They become smaller down to about 60 nm during the transition.

It was attempted to perform the same analysis on the diagrams obtained during oxidation at lower temperatures (800–1050 °C) and subsequent cooling. In that case, the surface oxide is always biphasic and it becomes very difficult to perform unambiguous identification of the lines. This makes the analyses very tedious but this mainly leads to less precise results. Some tendencies are reported in Figs. 9 and 10. The cell parameters of the phases are nearly constant on the whole studied oxidation temperature range. Moreover, these values are very close to those deduced at the same temperatures during cooling from 1100 °C (Fig. 7). High strains are then induced in the biphasic oxide. As an example,

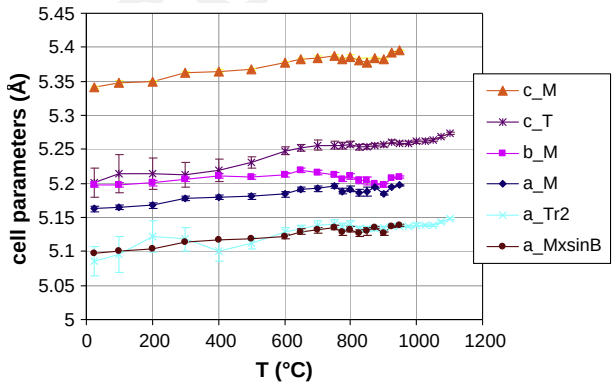

Fig. 7. Cell parameters of the oxide for an oxidation at 1100 °C of a Zy4 sample then cooled to room temperature.: a_Tr2: $a_T\cdot\sqrt{2}$. a_M × sin$B$: aM · sinβ. M, T: resp. monoclinic, tetragonal. Errors bars: ±2σ from Rietveld FPM refinements.

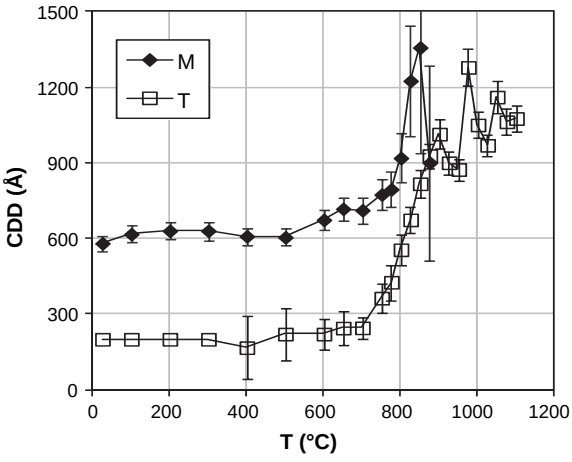

Fig. 8. Size of the coherent diffraction domains of the tetragonal (□) and monoclinic (■) phases after oxidation at 1100 °C then cooling to room temperature for a Zy4.

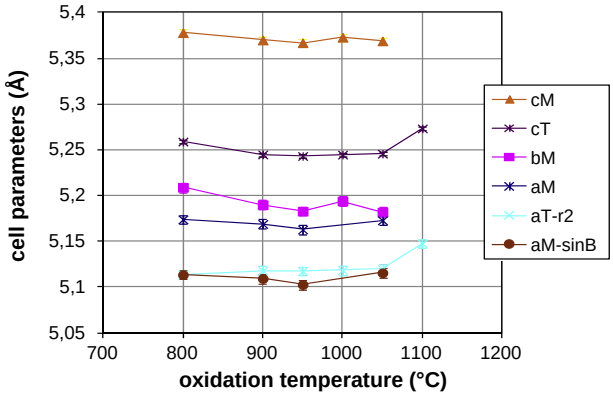

Fig. 9. Cell parameters of the oxide as it forms at the oxidation temperature for a Zy4 sample (same notations as in Fig. 7).

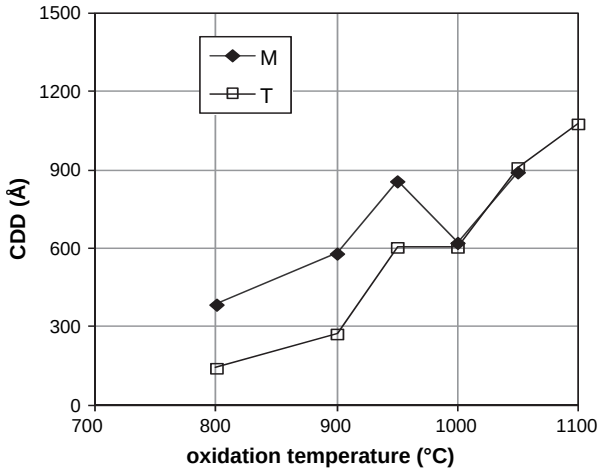

Fig. 10. Size of the coherent diffraction domains of the oxide T (□) and M (■) phases at the oxidation temperature for a Zy4 sample.

the cell parameters of the tetragonal phase are very different at 1100 °C, at which the oxide is purely tetragonal, and at 1050 °C, at which a mixed oxide forms. Topotaxic relationships between the a_M and b_M and a_T parameters similar to those obtained during cooling from 1100 °C and illustrated in Fig. 7 are observed.

As already observed during the cooling of the Zy4 sample oxidized at 1100 °C (Fig. 8) and as shown in Fig. 10, the CDD of the T and M phases have the same size during oxidation at high temperature (⩾1000 °C typically). Furthermore, the CDD are larger for the M phase than for the T phase when the oxidation is performed at lower temperature (Fig. 10). However, for both M and T phases, the domains are smaller during oxidation at a given temperature than after cooling from 1100 °C at this same temperature (e.g. at 800 °C, 30 nm *vs* 80 nm for the M phase domains and 20 nm *vs* 50 nm for the T phase ones). This may be due to the fact that the size of the crystallites at a given temperature is not the same when it results from the nucleation and growth mechanisms during the oxidation or when recrystallization or fragmentation mechanisms are involved during cooling from a higher temperature.

4. Discussion

The analyses reported in this paper have been performed in a temperature range (800–1100 °C) typical of LOCA conditions. It appears first that the composition and the microstructural properties of the oxide as it forms at high temperature drastically depend on the temperature: the oxide is purely tetragonal at the highest investigated temperature, mostly monoclinic at 800 °C and composed of both phases at intermediate temperatures (Fig. 6). Moreover, the oxide phases undergo high stresses leading to unusual cell parameters ratios. These stresses originate first from structural mismatches with the underlying metal (α-Zr(O) phase) then from topotaxic relationships between the two zirconia phases. The latter effect clearly appears for example in Fig. 7 but the former cannot be estimated here since the depth analyzed by the X-ray diffraction method is limited to about 5 μm: the metal becomes invisible rather quickly during the oxidation. This is clearly the strongest limitation of the method.

In the temperature range in which a mixed oxide is observed, the cell parameters of M and T phases show unusual variations: the usual evolution as a function of temperature is impeded by the interphases stresses (T and M ZrO_2, metallic substrate), during both cooling (Fig. 7) and oxide growth (Fig. 9). However, one should note that the oxide grains which are here analyzed have specific orientations, each different for a given diffraction line, given by the diffraction vector: due to the highly textured structure of the oxides, those data cannot be directly used to evaluate the actual, anisotropic, stresses undergone by the oxide. From Fig. 7, the thermal expansion coefficients of the cell parameters can be deduced (Table 2). In the temperature ranges in which they show a linear variation, the values obtained here are very close to those determined by Simeone et al. on a pure zirconia powder [7]. Only the b_M parameter thermal expansion shows significantly different values. This means the strain relaxation occurs somewhat differently in the oxide scale and in free powders.

The fractions of the monoclinic and the tetragonal phases are here estimated mainly from the ratio of the intensities of the main lines of the two phases. This is certainly a coarse approximation but it appears to be rather correct here. As an illustration, it is shown in Fig. 3 that the phase fractions estimated from the ratio of the main lines intensities are consistent with those evaluated with the full-pattern-matching method. However, this should be confirmed by performing further analyses, such as texture analyses during cooling; this would require setting a furnace on a texture goniometer.

The use of an asymmetric setup leads to specific effects as compared to a classical Bragg–Brentano one. The main one is that the grains contributing to the different lines of the diagrams are differently oriented relative to the surface of the sample. As a result, each line corresponds to a given orientation of a given population of grains which are all differently oriented. The formal consequence of this is that the cell parameters and the domains characteristics may differ from one line to the other, making any global analysis impossible. A first evaluation of this effect was attempted. The Zy4 sample oxidized at 1100 °C was analyzed on a Bragg–Brentano configuration at room temperature. The monoclinic phase was mainly observed, with a small tetragonal residue in accordance with the analyses performed on the asymmetric setup. A full-pattern-matching analysis of the diagram was then

Table 2
Thermal expansion coefficients ($K^{-1} \times 10^6$) of the cell parameters of the T and M phases in the temperature (°C) ranges in which their variations are linear as a function of temperature. Comparison between the results deduced from data illustrated in Fig. 7 for an oxide formed at 1100 °C on a Zy4 sample and from Simeone et al.' data for zirconia powder [7].

$K^{-1} \times 10^6$	a_M	b_M	c_M	a_T	c_T
This study	8.0	6.0	12.0	10.0	11.5
Temp. range (°C)	20–800			20–1200	
Simeone et al.	7.2	2.2	12.6	10.8	13.7
Temp. range (°C)	20–1200			1200–1600	

performed: the evaluated cell and linewidths parameters are very close to those obtained with the asymmetric setup. It then appears that the setup effect is of low consequence here, at least for the monoclinic phase at room temperature. This should be further investigated in particular at high temperature, here also by using a texture goniometer equipped with a furnace.

The oxide phase proportions reported in this paper, either during cooling or during oxide growth, are highly different from those expected from the known zirconia phase diagram [7]. In particular, high tetragonal phase fractions are stabilized at very low temperature. As mentioned in the Introduction, it is well known that the tetragonal phase of zirconia can be stabilized by stresses (whatever their origin: strain, point defects, surface energy,...), non-stoichiometry and/or addition elements. The tetragonal grain size estimated here after cooling is close to the one observed on free, pure zirconia grains, under which the high energy surface of the small grains allows a stabilization of the tetragonal phase down to room temperature [10,11]. Then it can be assumed that in the present case the tetragonal phase is stabilized at low temperature mainly thanks to a grain size effect (the impurities of the metal could also contribute to the stabilization). The crystal size under which the tetragonal phase is stable increases with increasing the temperature and tetragonal crystals becomes stable whatever their size above the T–M transition temperature. At high temperature, the grain size of the tetragonal phase is mainly controlled by the nucleation and growth mechanisms of the oxide at the metal surface, leading to large domains, about 110 nm for Zy4 at 1100 °C. When those grains are cooled, they become unstable and undergo both fragmentation and transition to the monoclinic phase. This transition leads to monoclinic variants which orientations are highly constrained by the pristine tetragonal grain orientations [22]. Then the first monoclinic domains should have nearly the same size as the largest tetragonal ones, as we deduce here. Further cooling may lead to additional fragmentation and/or to a transition into the monoclinic phase of the remaining tetragonal grains but the apparent size of the monoclinic domains remains high since the largest monoclinic grains are stable and the small grains only contribute to the feet of the diffraction lines, which are here poorly defined. These assumptions should be checked by looking at the oxide, by transmission electron microscopy for example, but one difficulty is that the T–M transformation is irreversible. When oxidation is performed at lower temperature, on the one hand, the tetragonal grain size results from a balance between the nucleation and growth mechanisms and the surface energy effect. On the other hand, two different populations of monoclinic grains are expected, one resulting from the first oxidation step, the other one resulting from the T/M transition during cooling. As mentioned above, the resolution of both the diagrams and the Hall–Williamson method does not make it possible to differentiate the two populations.

The values of the cell parameters suggest that strong topotaxic relationships exist between the oxide phases: the monoclinic a_M parameter is nearly equal to the tetragonal a_T one, modulo the geometric corrections, and the monoclinic a_M and b_M parameters are closer than usual. Such relationships between the T and M parameters have already been observed [22]. This can easily be understood when the monoclinic phase results from the T–M transition during cooling (Fig. 7) but these relationships are also observed during oxidation for all the oxidation temperatures investigated here (Fig. 9). One can then assume that the growth of the monoclinic phase is always controlled by a fraction of the tetragonal phase: this could be attributed to the presence of a tetragonal phase layer at the metal surface whatever the temperature, as already observed for oxidation performed at lower temperatures typical of normal conditions in LWR [20,28]. On the other hand, the ratio between the monoclinic a_M and b_M parameters reaches the usual value when the tetragonal phase proportion becomes low: as long as the tetragonal phase is predominant, the topotaxic stresses prevent normal stress relaxation. This should induce the formation of different variants of the monoclinic phase in the grains in order to limit the global angular distortion of the monoclinic grains. This can for example clearly be seen on the high resolution observations performed by Park et al. [29] where twins with large angular distortions are observed in the monoclinic grains. The orientation relationships between the T and M phases could be further studied by performing, for example, high temperature texture or electron backscatter diffraction analyses.

The results discussed in this paper may contribute to a better understanding of the high temperature oxidation of zirconium alloys under steady state or transitory conditions, in a general point of view or more specifically regarding particular phenomena such as the breakaway oxidation or the steam pressure effect (on Zy-4 for example) which generally occur at temperatures below 1050 °C. At these temperatures, it was shown that the growing oxide is composed of mixture of monoclinic and tetragonal phases (at atmospheric pressure), in a proportion which depends on the temperature. Gradients of phase composition can exist within the oxide, due for example to stress [20], grain size, micro-chemical, or temperature gradients either in steady states or in transient conditions. Furthermore, under these conditions, the metastable tetragonal phase may be locally destabilized during the oxidation. Since the tetragonal to monoclinic phase transition is associated with large distortions and volume changes [30], this would induce additional stresses and formation of pores or even cracks within the oxide which could cause breakaway oxidation for example.

5. Conclusions

In-situ X-ray diffraction structural and microstructural analyses of the oxide layer forming at high temperature (800–1100 °C) on Zircaloy-4 and M5™ alloys were performed. It was confirmed that the volume fraction of the tetragonal and monoclinic zirconia phases formed during oxide growth drastically depends on the oxidation temperature, e.g. the few outer microns of the oxide are fully tetragonal above 1050 °C and contain only 20% of tetragonal phase at 800 °C. The results obtained for Zircaloy-4 and M5™ are not significantly different. The oxide phase composition (tetragonal versus monoclinic) mainly depends on the size of the tetragonal phase domains. As deduced from the martensitic properties of the tetragonal–monoclinic phase transition, this grain size is mainly controlled by the interplay between the surface energy of the grains and the temperature. As a consequence, both the grain size (as estimated by the coherent diffracting domain size) and the phase proportion are irreversibly modified during cooling after oxidation. Therefore the observations performed post-facto either at room temperature or after re-heating to the former oxidation temperature cannot show the actual structure and microstructure of the oxide as it forms at high temperature. The proportion of tetragonal and monoclinic phases is obviously wrong, but, overall, the microstructure (texture, grain size, stresses) is different. Therefore the mechanisms and properties that depend on the oxide microstructure, such as oxide micro-cracking or gas diffusion through the oxide, cannot directly be deduced from post-facto observations.

Acknowledgments

This study was performed at CEA in the framework of the CEA-EdF-AREVA agreement. The authors thank Areva-NP and EDF for their financial contribution to this work. Areva-NP is also acknowledged

for material supply. We are deeply indebted to Jean-Luc Béchade for much interesting discussions and suggestions.

References

[1] K. Park, K.P. Kim, T.G. Yoo, K.T. Kim, Met. Mater. Int. 7 (2001) 367.
[2] M. Le Saux, V. Vandenberghe, P. Crébier, J.C. Brachet, D. Gilbon, J.P. Mardon, A. Cabrera, P. Jacques, in: 17th Int. Symp. Zirconium in the Nuclear Industry, ASTM STP 1543, 2013.
[3] S. Leistikow, G. Schanz, Nucl. Eng. Des. 103 (1987) 65.
[4] L. Portier, T. Bredel, J.C. Brachet, V. Maillot, J.P. Mardon, A. Lesbros, J. ASTM Int. 2 (2005).
[5] J.H. Baek, Y.H. Jeong, J. Nucl. Mater. 372 (2008) 152.
[6] P.M. Kelly, M.R. Francis-Rose, Prog. Mater. Sci. 47 (2002) 463.
[7] D. Simeone, G. Baldinozzi, D. Gosset, M. Dutheil, A. Bulou, T. Hansen, Phys. Rev. B 67 (2003) 064111.
[8] T. Nakayama, T. Koizumi, J. Jpn. Inst. Met. 31 (7) (1967) 839–845.
[9] P. Li, I.W. Chen, J.E. Penner-Hahn, J. Am. Ceram. Soc. 77 (1) (1994) 118–128.
[10] R.C. Garvie, J. Phys. Chem. 82–2 (1978) 218.
[11] G. Baldinozzi, D. Simeone, D. Gosset, M. Dutheil, Phys. Rev. Lett. 90–21 (2003) 216103.
[12] I. Kasatkin, F. Girgdies, T. Ressler, R.A. Caruso, J.H. Schattka, J. Urban, K. Weiss, J. Mater. Sci. 39 (2004) 2151–2157.
[13] D. Simeone, G. Baldinozzi, D. Gosset, S. LeCaër, L. Mazerolles, Phys. Rev. B 70 (2004) 134116.
[14] S. Block, J.A.H. Da Jornada, G.J. Piermarini, J. Am. Ceram. Soc. 68–9 (1985) 497–499.
[15] B. Cox, J. Nucl. Mater. 336 (2–3) (2005) 331–368.
[16] D. Gosset, M. Le Saux, D. Simeone, D. Gilbon, J. Nucl. Mater. 429 (2012) 19–24.
[17] Ch. Valot, D. Ciosmak, M.T. Mesnier, M. Lallemant, Oxid. Met. 48-3-4 (1997) 329.
[18] D. Simeone, D. Gosset, G. Baldinozzi, J. Appl. Cryst. 46 (2013) 93–98.
[19] M. Le Saux, J.C. Brachet, V. Vandenberghe, D. Gilbon, J.P. Mardon, B. Sebbari, Influence of pre-transient oxide on LOCA high temperature steam oxidation and post-quench mechanical properties of zircaloy-4 and M5™ cladding, in: 2011 Water Reactor Fuel Performance Meeting, Chengdu, China, September 11–14, 2011.
[20] J. Godlewski, in: *X*th Int. Symp. Zirconium in the Nuclear Industry, ASTM STP 1245, Baltimore, MD, 1994, pp. 663–684.
[21] G. Schanz, B. Adroguer, A. Volchek, Nucl. Eng. Des. 232 (2004) 75–84.
[22] J. Chevalier, L. Gremillard, A.V. Virkar, D.R. Clarke, J. Am. Ceram. Soc. 92 (9) (2009) 1901–1920.
[23] Ch. Valot, D. Ciosmak, M. Lallemant, Solid State Ionics 101–103 (1997) 769–774.
[24] J.F. Berar, P. Garnier, in: APD II Conference, 26–29 Mai, NIST, Gaithersburg, MD, USA, 1992.
[25] D. Simeone, G. Baldinozzi, D. Gosset, G. Zalczer, J.F. Bérar, J. Appl. Cryst. 44 (2011) 1205–1210.
[26] The Rietveld method, in: R.A. Young (Ed.), IUCr Monograph on Crystallography, Oxford Univ. Press, 1993 (No. 5).
[27] S. Deville, G. Guénin, J. Chevalier, Acta Mater. 52 (2004) 5697–5707.
[28] N. Pétigny, P. Barberis, C. Lemaignan, Ch. Valot, M. Lallemant, J. Nucl. Mater. 280 (2000) 318–330.
[29] D.J. Park, J.Y. Park, Y.H. Jeong, J.Y. Lee, J. Nucl. Mater. 399 (2010) 208–211.
[30] E.H. Kisi, C.J. Howard, Key Eng. Mater. 153 (1998) 1.